Molecular simulation of thermoset curing: application to 3D printing materials

Márk Jenei[a], Reinier L. C. Akkermans[b], Struan Robertson[b], James A. Elliott[a,*]

[a]Department of Materials Science and Metallurgy, 27 Charles Babbage Road, University of Cambridge, Cambridge, CB3 0FS, United Kingdom

[b]Dassault Systèmes BIOVIA, 334 Cambridge Science Park, Cambridge, CB4 0WN, United Kingdom

ARTICLE HISTORY

Compiled September 9, 2020

ABSTRACT

Two methods have been developed for the simulation of arbitrary polymerisation processes and the construction of large-scale 3D polymer networks. The first builds on the idea of cutoff distance-based reaction handling in a Molecular Dynamics environment, while the second utilises a scheme that pulls together monomers that are to react, significantly lowering the required computation time, but still ensuring the correct physical evolution of the polymer network. The protocols were used to model a compound bismaleimide material used in 3D printing, and its thermomechanical properties were compared with experimental results.

KEYWORDS

3D printing, molecular dynamics simulation, polymerisation, COMPASS III, thermoset curing

1. Introduction

Conventional three-dimensional (3D) printing uses a feedstock of pellets or filaments made of thermoplastic material that can be melted and extruded before solidifying

*Corresponding author. E-mail: jae1001@cam.ac.uk

into their final shape. 3D printing of thermosetting polymers, however, represents a much greater challenge, as these materials cannot be melt-processed and so need to be cured during or after printing to retain their shape, over times that generally exceed those of the rapid 3D printing process. Yet, being able to print thermosets is highly desirable due to certain beneficial properties these materials offer over thermoplastics, such as thermal stability and chemical resistance, and the costs and energy-intensity of the traditional moulding process used to fabricate 3D architectures.

Recent advances in additive manufacturing technology[1] have enabled 3D printing of certain thermoset systems such as polyether-ether-ketone[2], polyimides,[3], polyurethanes and epoxy resins.[4,5] These typically use highly-reactive photocurable resins with fillers to thicken and reinforce the inks. The ability to customise 3D architectures with precise control over microstructure results in a significant potential for innovation in many fields including microelectronics, biomedical engineering, microfluidic devices and soft robots.[6]

Bismaleimide (BMI) resins are a class of high-performance thermosetting polymers that have recently been used in 3D printing.[7–10] BMI resins have excellent chemical and thermal stability and outstanding mechanical properties, making them attractive for industrial applications. BMI monomers consist of an alkyl or aryl group connecting two maleimide groups that can undergo a range of addition-type chemical reactions, such as ene and Diels-Alder reactions. BMIs will polymerise at high temperatures, resulting in highly crosslinked networks. Consequently, BMIs tend to be brittle and are often co-polymerised to improve their fracture toughness.

The material properties of thermosetting polymers are strongly dependent on both the detailed molecular structure of the constituent resin and cross-linker monomers and on the topological properties of the polymer molecules formed during the curing process. There is a great demand for tailoring properties of thermosets, but there are significant challenges in the detailed understanding of these materials using conventional experimental methods. Amongst these challenges is the lack of direct access to the structure of the polymer network on the length scale of monomers. To complement experimental methods, computer simulations of the polymerisation process can be used. Although these depend on the selected model chosen for the

simulation, they provide detailed information on the topological evolution of the system in the polymerisation process, which can lead to a better understanding of the structure-property relationship, with potential to guide materials design.

Molecular simulations have been used extensively in the modelling of thermosetting polymers, especially the curing process of epoxy resins. Various thermomechanical properties were calculated for epoxy-amine co-polymers, such as the modulus [11], the glass transition temperature [12,13] and the relationship between microstructure and material properties [14]. Fu *et al.* calculated the thermomechanical properties and the effect of microstructure for an acid anhydride-epoxy system [15].

In this work, we report on molecular simulations of BMI network formation using BIOVIA Materials Studio 2020[16]. The bismaleimide model system is described, and two methods for constructing polymer network models are introduced; *Reactive Molecular Dynamics* and *Guided Reactive Molecular Dynamics*, the first of which builds on well-established ideas [17–20] and the user-friendly graphical interface of Material Studio, whilst the second can reduce the required CPU time to build polymer models by a factor of four, compared to the former method.

These methods are used to build polymer networks for four different compositions of the model 3D printing material. After verifying that the guided approach results in physical networks, two Material Studio protocols (described below) were used to measure the glass transition temperature and the stress-strain properties of the constructed polymer models, and the results were compared with experimental data.

2. Methods

2.1. Model system

We consider traditional BMI mixtures of *N*,*N*'-(4,4'-Diphenylmethane)bismaleimide (BDM) and diallylbisphenol A (DBA), which are copolymerised at high temperature to obtain a BDM/DBA pre-polymer. The reaction proceeds via an ene reaction, where the allylic hydrogen in DBA transfers to the enophile moiety in BDM shifting the double bond to the allylic position. To the liquid pre-polymer, *N*-vinyl-2-pyrrolidone

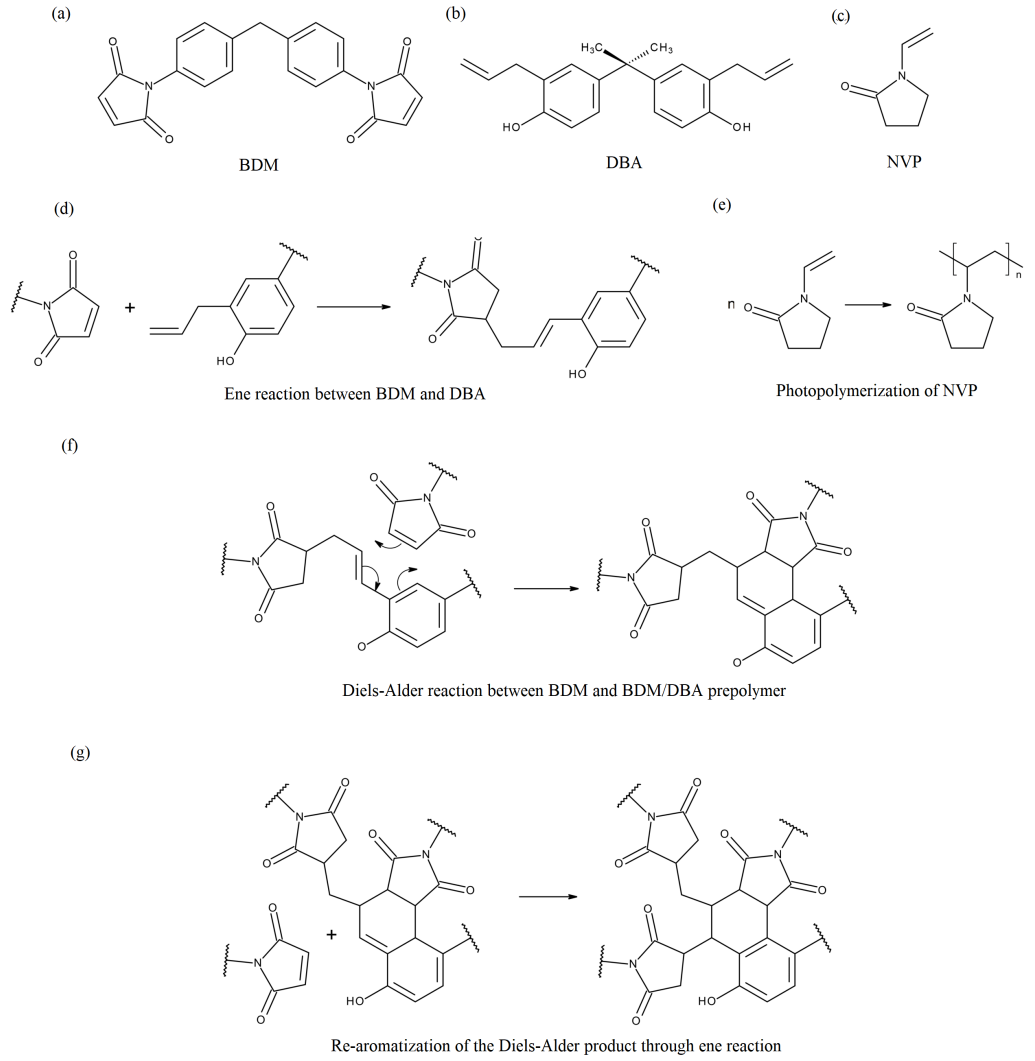

Figure 1.: Compounds used in this study: (a) *N*,*N*'-(4,4'-diphenylmethane)bismaleimide (BDM), (b) diallylbisphenol A (DBA), and (c) *N*-vinyl-2-pyrrolidone (NVP). Reactions (d) and (e) proceed in the first phase of the curing process, while reaction (f) and (g) occur during the thermal process of crosslink formation.

(NVP) is added as a reactive diluent, together with a photoinitiator. This constitutes the BMI ink for 3D printing.[7] In the simulation study, we ignore the photoinitiator compound and perform the copolymerisation in the presence of NVP, with a predefined number of monomers having been initiated and possessing a reactive carbon atom with a free radical electron. The monomers and their reactions during the curing process are shown in Fig. 1.

The curing of the physical material takes place in two stages: NVP is added to the liquid prepolymer containing BDM/DBA chains in order to solidify the deposited ink through photopolymerisation induced by UV radiation. In a second stage, the printed samples undergo heat treatment, which promotes the curing of the prepolymer through the Diels-Alder reaction. This is followed by a re-aromatisation via the ene reaction (bottom of Fig. 1), resulting in a material with an underlying crosslinked network structure.

2.2. Reactive Molecular Dynamics

Reactive Molecular Dynamics (RMD) simulates the curing process by running MD simulation on the polymer system, and the run is periodically interrupted to check for possible reactions. MD is expected to be capable of accurately modelling the diffusion process, within the limitations of the force field used, and the effect of the relatively small simulation cell size. Below is an outline of the methods used to handle reactions in this protocol, summarised in Fig. 2.

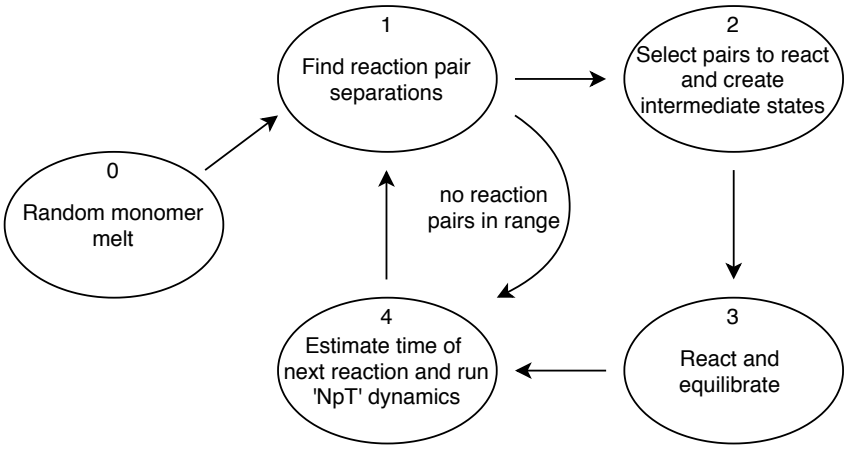

Figure 2.: Flow chart of the RMD protocol.

1. Reactions are defined by specifying the fragments of reactant monomers that change in the reaction, along with the reaction-initiating atoms on each fragment. Using the graphical interface of Material Studio, it is possible to avoid the often tedious process of pre- and post-reaction topology specification (see Appendix B). In reaction checks, the system is scanned for molecule fragments that match the configuration of

the reactants as defined in the reaction document, and the reaction atoms on these are located. Having obtained the lists of reaction atoms, the 3D separation between them is calculated. If this separation is below a predefined threshold, the pair is accepted to react with a set probability.

2. Once the system is scanned for reactions, the algorithm constructs intermediate states for each accepted reaction pair. Strong attractive harmonic potentials are introduced between the atoms that are to form bonds in the reaction. To bring these atoms closer together, and to create an intermediate geometry for the reacting fragment, a geometry optimisation routine is used. The reacting fragment is relaxed using conjugate gradient optimisation for 5 steps, and the separation of all atoms that are to from bonds is calculated. If all the distances are below 3 Å, the intermediate states are formed. If not, another optimisation cycle is run. Atoms which are not part of the reacting fragments are fixed to avoid the interruption of the overall dynamics simulation.

3. After the intermediate states are formed, the harmonic potentials are replaced by bonds, and the bonds that break in the reaction are removed. This results in large changes in the energy of the atoms that are part of the reacting fragment. To equilibrate these, and remove internal stresses and geometry distortions, the subsystem containing the atoms participating in the reaction undergoes two cycles of short NVE dynamics (50 steps with 0.1 fs timestep) followed by geometry optimisation (5 cg steps). As before, all atoms that are not part of the reacting fragments are kept fixed. The atomic charges are updated according to their new force field type.

4. Following the update of molecular topology and equilibration, the algorithm returns to the NpT dynamics simulation of the system for a given number of timesteps. Since a reaction check is an expensive procedure, it is desirable to avoid frequent interruption of the simulation, but still ensure that most of the possible reactions are spotted. To find a trade-off, the number of steps used for the dynamics simulation in a given cycle is calculated by the mean-squared displacement (MSD) of reactive atoms in the previous run, and the current lowest separation of a possible reaction pair. Using the MSD calculated over the last dynamics run, an average speed of the reactive atoms can be defined. Dividing the lowest separation by this speed gives an

estimate of when the next reaction might occur. The time of the next reaction check is set accordingly.

2.3. Guided Reactive Molecular Dynamics

2.3.1. Motivation

In theory, the RMD method is capable of generating physically realistic polymer networks within the accuracy of the current general MD models and the supplied parameters. However, in a realistic case, the diffusion of the atoms decreases quickly with increasing degree of conversion, and the simulations become very time-consuming due to the required length of the dynamics runs that enable unreacted atoms to diffuse within the reaction range.

If it were possible to predict which atoms will react, these could be guided towards each other. A promising theoretical model for the evolution of molecular networks is chemical Random Graph Theory (RGT).[21–23] In RGT, the topological evolution of the molecular network is described by a process on a mathematical graph which evolves by adding edges between nodes, representing the bonds and monomers respectively. A graph is essentially a two-dimensional mapping of the connectivity pattern of a network, with no regards to spatial information. The dynamics of the graph at given a conversion can be captured by specifying how nodes are selected in the polymerisation process to form new edges.

In the ideal polymerisation approximation, it is assumed that reactivity of the *functional groups* is independent of monomer degree, i.e. their reactivity will not decrease as the monomer it resides on forms bonds with other monomers. In this case, the monomer reactivity ($r(n)$) is proportional to the number of its free degrees that is the number of groups not yet reacted:

$$r(n) = m - n \tag{1}$$

where m is the maximum number of bonds the monomer can form, and n is its degree.

Using this approximation in the graph description of polymer networks, the prob-

ability of selecting a node for the next reaction will be proportional to its free degrees. A simple graph simulation would then calculate the probability of the selection of each node as a function of their degrees, and use these as weights. This weighted probability distribution then can be used to choose a pair of nodes to form the next edge.

As found by Kryven [24], for systems that undergo ideal polymerisation, it is possible to derive the expected degree distribution, u, over the process and is given by:

$$u(n, m, t) = \binom{m}{n} c^n(t)\big(1 - c(t)\big)^{m-n} f_m \tag{2}$$

where n and m are the current degree and functionality of the node respectively, f_m is the initial fraction of monomers with functionality m, and c is the conversion of functional groups, which is a function of time. In essence, u gives the probability at a given conversion that a randomly selected node on the graph with given functionality has formed n edges.

2.3.2. Protocol

In the case where a system undergoes polymerisation in which the degree distribution evolves as given above, it can be assumed that this process is modelled accurately with the random graph approach. Having obtained a good description of the dynamics of the system, it might now be possible to predict its topological evolution and use this to accelerate simulations. Returning to the idea of GRMD, a direct translation of the ideal polymerisation process would be to randomly select appropriate atom pairs for reaction and introduce attractive potentials between them, so that the diffusion of the reacting functional groups towards each other is faster.

The assumption of ideal polymerisation is included in the selection process, as it is the functional groups on a monomer rather than the monomer itself that is chosen for the reaction. The more reactive functional groups a given monomer has, the higher the probability that this monomer is selected.

In case the system's evolution is different from the ideal case, a modified version of GRMD can be used to construct realistic networks. Deviation from the ideal evolution

manifests itself with a change in the degree distribution at a given conversion. If this distribution is known, it is possible to select reaction pairs, such that at the end of the simulation at the given conversion, the monomer's degree distribution will match the expected one.

For the newly introduced attractive potentials, a harmonic is used with a force constant so that the quarter of a period of oscillations of each pair is equal to the timestep. A harmonic force was chosen, so that reaction atoms further apart would not require much more time to reach each other's vicinity, but other attractive potentials could also be used.

Introducing the new attractive harmonic potentials results in an increase in the energy of the system, moving it further from equilibrium. The larger the separation of atoms restrained by the new attractive potentials, the higher the sudden increase in energy. To minimise this effect, instead of selecting the reacting functional groups truly randomly, the current distance between all possible reaction pairs is calculated with regards to the periodicity of the simulation cell, and potentials are introduced between atoms with the shortest separations.

For the modified version, where the ideal polymerisation is expected not to hold, a similar approach is used. However, as iterating through the list of possible reaction pairs, from shortest to longest, it is checked whether the newly introduced bond would not violate the expected degree distribution. If it is the determined by the degree distribution, that at the target conversion c_t, the number of n degree monomers should be $N(n, c_t)$, and the monomer forming the proposed new bond would be the $(N+1)^{th}$ with degree n, the new bond is rejected.

Depending on the nature of the polymerisation process, the harmonic potentials are introduced differently. For step-growth polymerisation, all functional groups are able to react throughout the process, unless they have already done so. For this case, all of the future reaction pairs can be found before the simulation, according to their initial separation, and the atoms of these pairs can be restrained by harmonic potentials. The number of new potentials is such that after all restrained pairs have reacted, the desired conversion is reached.

In free radical polymerisation, the same approach cannot be used: the reacting

capabilities of the monomers change because a pending double bond (PDB) transforms into a free radical on a monomer following propagation reactions. Here, the restraints are instead introduced in cycles. Initially, the attractive harmonic potentials are introduced between atoms with free radicals and their closest reaction pair, which can be either another free radical atom, or one with a PDB. Once one such atom becomes within range of its pair, the reaction is performed, and in case of propagation reactions, the new radicals are restrained with their closest reaction pair. The process is continued until the required degree of conversion is reached, or no more radicals are present in the system.

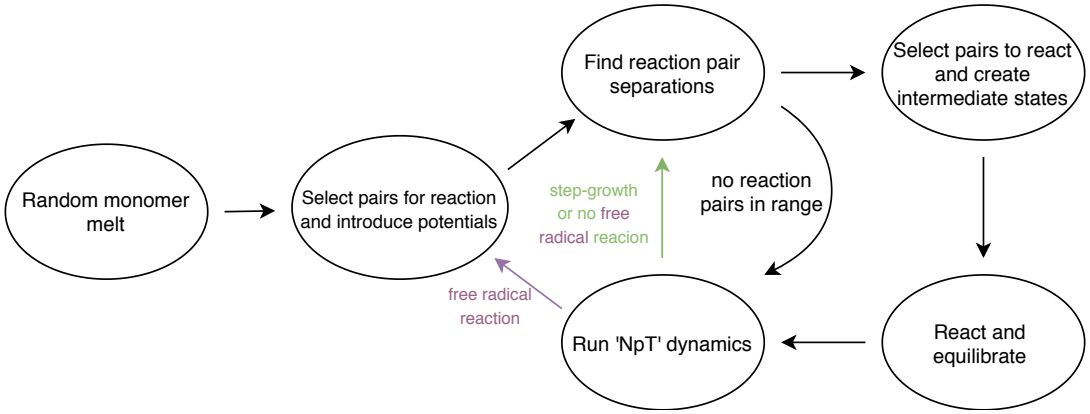

Figure 3.: Flow chart of the GRMD protocol.

Apart from the introduction of the attractive harmonic potentials in the system, the GRMD protocol uses the same methods that are used in RMD above described, as shown in Fig. 3.

2.4. Physical properties measurements

After the simulation of the curing process, 10 samples were randomly chosen and were equilibrated in preparation for analysis. The equilibration consisted of geometry optimisation using Materials Studio's "Smart Algorithm", with a convergence condition for the energy change of $1x10^{-4}$ kcal/mol, followed by 100 ps of NVT dynamics using the velocity-scaling thermostat set at 298 K. This was proceeded by another 1 ns of NpT dynamics using the Nosé-Hoover-Langevin (NHL) thermostat and Andersen barostat, set at 298 K and 1 atm respectively. The above equilibration process is expected to

remove all residual stresses from the production simulations. The prepared structures were then used as inputs to a simulated dilatometry protocol, to determine the glass transition; and a tensile test protocol to obtain the stress-strain diagram. Monomers that are not part of the final infinite polymer network are kept in the simulation cell, to account for the caging effect present in realistic materials.

In dilatometry, the sample is heated up to a high temperature and cooled in stages. At each temperature during cooling, the volume is measured. The variation of volume over all samples at each temperature is determined as the standard error of the mean. The data set is then fitted to a non-linear function to obtain the glass transition temperature, as well as the thermal expansion in the glass and rubber state, as detailed in Appendix A. The protocol was run in the temperature range 1000-200 K, decreasing in steps of 80 K. Each step consists of 50 ps equilibration and 350 ps production, giving a cooling rate of 0.2 K ps^{-1}.

In the tensile tests, the samples are first simulated at normal temperature and pressure to determine the cell dimensions in the absence of load. The Souza-Martins barostat [25] was used, which allows the variation of all cell parameters independently. During this procedure the system was extended in small steps in the X-direction, and compressed in the Y and Z directions using an initial estimate for the Poisson ratio. The transverse stress (stress perpendicular to the tensile axis) was monitored, and if it exceeded a threshold, the Poisson ratio was adjusted such that the transverse stress remained within the threshold. This procedure simulates an experiment to measure the unconstrained Young's modulus under standard conditions.

At each strain, the average tensile stress was measured, and its variation over all samples at each point was determined as the standard error of the mean. Finally the stress-strain data were fitted to a non-linear function, to determine the Young's modulus, the yield stress, and the critical deformation. The protocol was run up to a strain of 20% in 10 steps. Each step consists of 100 ps of equilibration and 400 ps of production, giving a strain rate of 0.4 ns^{-1}. The initial Poisson ratio was 0.3, and the transverse stress threshold was set to 0.1 GPa.

2.5. Curing process simulation details

In the polymer network production runs, the prepolymer preparation (BDM-DBA chains), and the free radical polymerisation of NVP monomers are simulated simultaneously. The Amorphous Cell package of MS is used to construct the initial polymer melt containing the desired number of the three types of monomers, and using a target density of 1.0 g/cm^3, which is slightly below the physical density.

The constructed simulation cells are already geometrically optimised. To further equilibrate the system, and to achieve the expected true density, an NpT dynamics run is used for 25 ps.

This, and all other dynamics and geometry optimisation runs in the presented methods use the Forcite package of MS, and the COMPASS III force field. In all cases, the NpT simulations use a timestep of 0.5 fs, the Nosé thermostat with the temperature set to 413 K, and the Berendsen barostat - both with a decay constant of 0.1 ps.

Electrostatic and van der Waals forces are calculated using the Ewald and atom based summation, respectively, the former with accuracy 10^{-4} kcal/mol, and the latter with a cutoff of 15.5 Å. The Newton equations are integrated using the Verlet algorithm.

For each material, 20 polymer network models are constructed, each with a different random initial monomer melt. Otherwise, all simulation settings are identical: reaction are performed once the reaction initiating atoms are within 3 Å, the final conversion for the chain forming reactions (NVP and BDM-DBA) was set to 90%, and the crosslinking conversion was set to 100%.

2.6. Eligibility of GRMD

The functional groups on the BDM and DBA monomers are well separated on the molecule, and groups that have not yet reacted reside either on free monomers or on chain ends. Therefore, it is expected that the assumption of independent functional group reactivities holds, and the polymerisation process can be approximated as a random ideal polymerisation.

To confirm this, a mixture of BDM and DBA molecules were simulated using the RMD protocol. 104 BDM and 90 DBA monomers were distributed randomly in a periodic simulation cell with initial dimensions of 47.6 Å in each direction, and relaxed using NpT dynamics until the density and temperature fluctuations settled. After equilibration, 500 cycles of the RMD protocol were performed, using a threshold separation of 4 Å and a probability of 1.0 for reactions. Using a batch of 20 such samples, an average of 80% conversion was reached, which gives a large enough range to compare the evolution of the system with the ideal case.

3. Results

3.1. Degree distribution

The evolution of the degree distribution for the BDM/DBA systems, as found by the RMD simulations is shown in Fig. 4, along with the expected evolution based on RGT as given by Eq. (2).

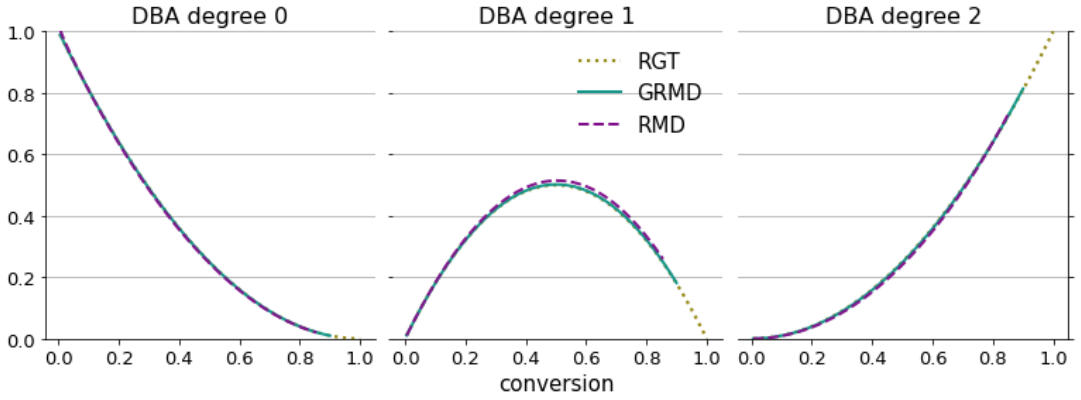

Figure 4.: Degree distribution of DBA monomers as a function of conversion as expected by Random Graph Theory (RGT), and as observed by simulations using the Reactive Molecular Dynamics (RMD) and the Guided Reactive Molecular Dynamics (GRMD) protocols.

As the distributions are almost identical, the random polymerisation model is expected to describe the system evolution correctly, and the original version of the GRMD protocol is applicable. To assure that the implementation of GRMD reproduces the ideal degree distribution, 20 test runs were performed on another batch of BDM/DBA melts, with the final conversion set to 90%. Other properties, such as the

reaction range or the number of molecules were left unchanged. The CPU time of these simulations dropped significantly to roughly 10 hours, compared to 60 hours using RMD. Reassuringly, the evolution of the degrees is identical to the RGT prediction and the results from RMD simulations, as shown in Fig. 4.

3.2. Cluster size

In the following, topological and physical properties of a set of BMI mixtures are examined. The weight ratios of BDM, DBA and NVP monomers in the simulation cell are set so that they match the samples used in the work by Wu *et al.* [7], as summarised in Table 1. In each case, 2.5% of the NVP monomers were initiated, possessing a carbon atom with a free radical on it.

Label	**BDM**	**DBA**	**NVP**	**NVP(initiated)**
BMI-1	104	90	162	4
BMI-3	104	90	244	6
BMI-5	104	90	325	8
BMI-7	104	90	406	10

Table 1.: Monomers in the simulation cell for the samples tested in this study, following the notation in [7]. In all cases, 2.5% of NVP monomers are initiated.

As described above, there are two main phases of the curing process: first in which BDM-DBA and NVP polymer chains are formed, and second the bonding of the BDM-DBA pre-polymer chains through crosslink formation. In this work, both of these phases are simulated using the GRMD protocol, and the evolution of the molecular size distribution is obtained (instead of the usual weight distribution, due to the finite size of the simulation box). A typical example of the molecules formed at the end of the two phases is shown in Fig. 5.

Using the first and second moments of the size distribution, the number and weight average molecular size can be found as a function of conversion. Fig. 6 shows the results for the size evolution throughout the complete curing process for each type of polymer.

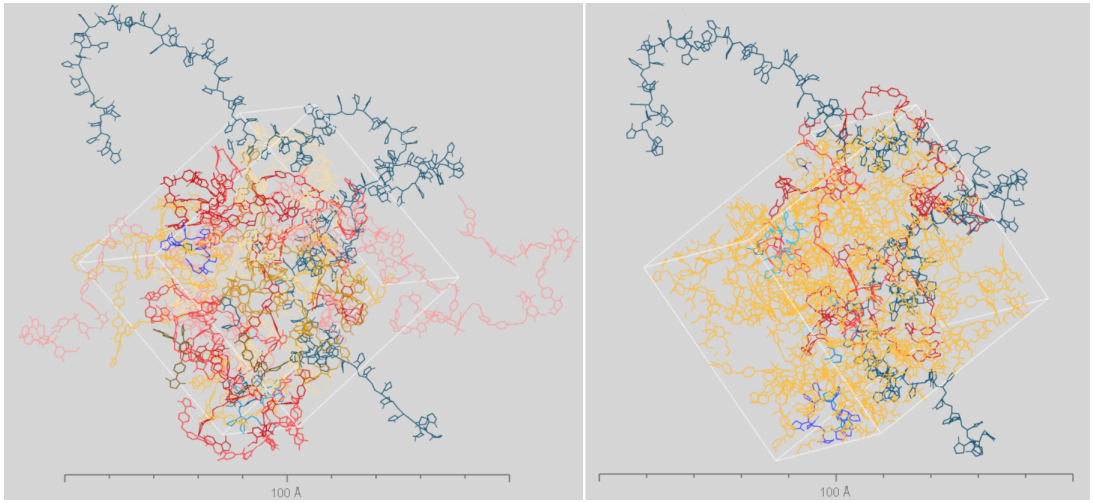

Figure 5.: A screenshot of the amorphous simulation cell before (left) and after (right) crosslink formation. NVP chains are coloured blue, finite BDM-DBA chains red or orange (left), and the infinite periodic giant BMI molecule orange (right). Finite molecules are displayed across neighbouring simulation cells so that they appear continuous.

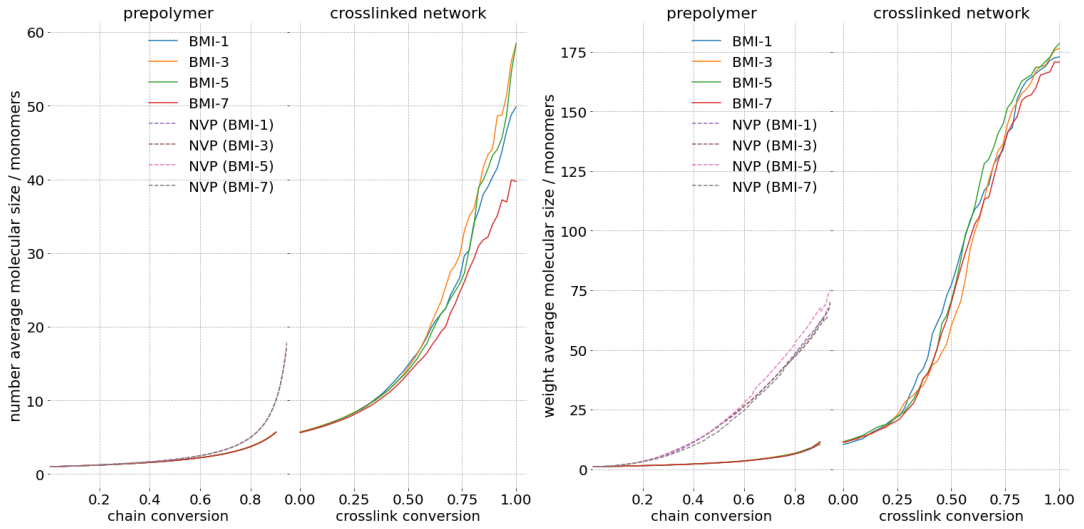

Figure 6.: Number (left) and weight (right) average molecular size as a function of conversion for BMI. The x-axis is divided according to the two phases of the curing process. First, the conversion stands for functional groups undergoing the ene and radical reactions, while the second part gives the conversion of groups participating in the crosslink forming reactions. Results shown are averages of 20 runs for each type of BMI/NVP polymer mixture.

As expected, the average size of NVP chains is larger in the pre-polymer phase, as here chains grow from a few initiated monomers resulting in a handful of very long polymeric molecules, whilst in the case of BDM-DBA, chains may start growing from

either of the monomers, resulting in a larger number of polymer molecules with similar, moderate sizes, hence the close values of the two different averages. Furthermore, it appears that the relative number of NVP monomers does not affect the formation of the BDM-DBA chains, and that the average size of NVP chains is also similar due to the identical percentage of initialised monomers used.

At the end of the chain forming pre-polymerisation process, there will be some free BDM monomers due to the initial excess concentration of them compared to DBA monomers. This explains the change in the gradient of the BMI cluster size curves, as first these free monomers bond to the BDM/DBA chains, only slightly increasing their size. The steep growth corresponds to gelation, where the excess BDM monomers that are already bonded to a chain start connecting to other ones, creating crosslinks.

The similar weight average molecular size curves of each BMI material indicate that the size evolutions of the largest macromolecules in the system are close to identical. On the other hand, the lower number average size for BMI-7 indicates the presence of smaller molecules, possibly monomers. This could be a result of the higher NVP concentration, and the caging of BDM/DBA monomers by the forming large NVP chains.

3.3. Thermomechanical properties

Once the simulated polymer networks were obtained, and the structures were equilibrated, the physical properties of the materials were measured using the *Calculate Glass Transition Temperature* and *Calculate Yield Stress and Critical Distortional Strain* protocols in Pipeline Pilot (see Sec. (2.4)), and the final cell densities were recorded for the shrinkage measurements. The outputs of these protocols are illustrated in Fig. 7, with data included only for some of the results.

3.3.1. Volume shrinkage

First, the volume shrinkage upon crosslinking was measured for each type of material, using the equilibration routine described in Sec. (2.4). The density is calculated after the pre-polymerisation, chain forming phase, and after crosslink formation. In Table 2

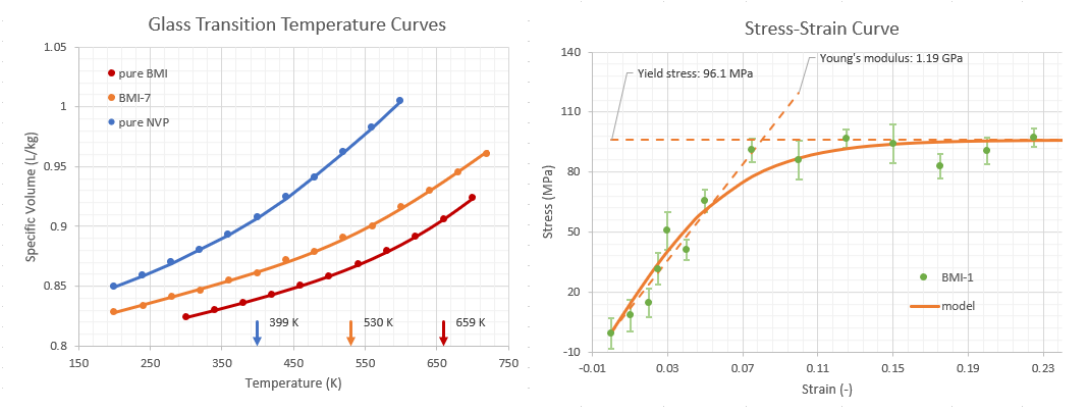

Figure 7.: Results of the *Calculate Glass Transition Temperature* (left) and the *Calculate Yield Stress and Critical Distortional Strain* (right) protocols. To find the final glass transition temperatures, the obtained results were subjected to WLF and Flory-Fox analysis (see Appendix A). Young's modulus is approximated as the gradient of the stress-strain curve in the range, where Hooke's law holds, while the yield stress is taken as its asymptotic value for large strains.

the densities and the one-dimensional shrinkage is shown. The shrinkage values are very

Material	ρ_{chains}	$\rho_{xlinked}$	1D shrinkage
BMI-1	1.13	1.20	1.8%
BMI-3	1.12	1.19	2.0%
BMI-5	1.11	1.18	2.1%
BMI-7	1.10	1.18	2.4%

Table 2.: The densities after the pre-polymerisation simulations (ρ_{chains}), after the crosslink formation ($\rho_{xlinked}$), and the one-dimensional shrinkage.

close to the ones found experimentally [7], where the shrinkage of a thin rectangular sample was measured. There, the shrinkage of the larger sides were found to be 2.0% and 2.2%, and 3.6% for the thin side, resulting in a total shrinkage of 2.6%.

3.3.2. Mechanical properties

Using the results of the tensile simulation protocol, the Young's modulus and the yield stress can easily be obtained from the stress-strain curves, as shown in Fig. 7. It is important to note that this protocol does not account for fracturing, and no bonds break in the stretching process. However, the breaking point in a physical experiment

and the point where the simulation cell starts to expand rapidly can be related, as this is the point where force fields (designed to model systems in equilibrium) break down, or the physical material fractures. Hence the yield stress obtained from simulation and the tensile strength observed in an experiment can be compared. Results for the mechanical properties of the simulated networks and values found experimentally for these BMI materials [7] are shown in Table 3.

Material	σ_y(MPa)	TS(MPa)	E(GPa)	E_{exp}(GPa)[7]
pure BMI	97.38	71	1.12	-
BMI-1	94.81	78	1.20	2.9
BMI-3	116.68	91	1.22	3.2
BMI-5	165.42	88	1.16	3.5
BMI-7	100.30	70	1.24	4.1
pure NVP	84.99	19.6	-	-

Table 3.: Comparison of mechanical properties of the simulated polymer networks, and experimental results[7]. Yield stress (σ_y) is compared with the experimental tensile strength (see text), while Young's modulus is obtained both from simulation (E), and from experiment (E_{exp}).

The yield stress - tensile strength comparison reveals that the tested materials have their highest strength at intermediate NVP contents, but the matching of trends is not good enough to deduce accurate prediction using the results of the simulations. The obtained Young's modulus values on the other hand deviate significantly from the expected values, by about a factor of 3. As pointed out in Ref. [26], where similar deviation was observed in measuring the Young's modulus for a thermosetting material, it might mainly be the result of the large difference in the straining rates in simulations and experiments. It is possible that crystallisation in the physical material that is not captured in the model also has significant effects, which could be experimentally tested using X-ray scattering. Additionally, it might be that the equilibration times were not sufficiently long, and the BMI/NVP entanglements could not have been adequately formed. Furthermore, in the stretching protocol, the small simulation cell is relaxed fully; this might only be true in a realistic case for the surface of the material but not in the bulk, where the material is confined by the outer layers.

3.3.3. Glass transition temperature

In determining the glass transition temperature, the limitations of the simulations can lead to some inaccuracies. Most importantly, these typically run on a timescale of nanoseconds, compared to a realistic cooling process that usually takes minutes. However, both the relatively rapid cooling rate and the finite size of the simulation box can be accounted for using extrapolation methods based on the Williams-Landel-Ferry (WLF)[27] and the Flory-Fox equations respectively. For the latter, number and weight average molecular sizes are used (see Sec. (3.2)), as suggested by Ogawa[28] (see Appendix A) for systems with a wide size distribution, as is the case for BMI/NVP copolymer system, while it is simply the number average size that is used for pure NVP. Table 4 shows the results of these simulations along with their corrections.

Material	T_g(K)	$T_{g,wlf}$(K)	M_n(kDa)	M_w(kDa)	$T_{g,final}$(K)	$T_{g,exp}$(K)[7]
pure BMI	659	552	1.33	26.72	597	615
BMI-1	549	442	5.15	45.84	460	469
BMI-3	548	441	4.80	43.04	460	483
BMI-5	546	439	3.92	39.92	461	459
BMI-7	530	423	3.41	35.79	447	401
pure NVP	399	291	2.38	7.12	357	373

Table 4.: Results of the glass transition temperature simulations (T_g), with the WLF correction ($T_{g,wlf}$), the number and weight average molecule weights used (M_n, M_w respectively) in the Flory-Fox equation, and the final T_g value with both the WLF and the Flory-Fox correction ($T_{g,final}$). Experimental values of T_g ($T_{g,exp}$) from Ref. [7].

Although the simulations fail to spot the spike in the T_g for BMI-3, they show similar trends with changing NVP content. With the corrections applied, all glass transition temperatures are found reasonably close to the expected values, with some room still left for further improvements in the accuracy of the obtained values.

4. Discussion

It is expected that for systems consisting of monomers on which the functional groups are well spaced, the assumption of ideal polymerisation holds. In this case, the monomer reactivity is proportional to the number of its unreacted groups, and their

reactions do not result in steric hindering or diffusion limitations of the monomers and their remaining unreacted functional groups.

To confirm this, RMD and GRMD simulation were run on a set of BDM/DBA melts. In RMD, the dynamics is controlled solely by the common forces of an MD simulation, making it possible to reveal accurate changes in monomer reactivity as a function of its topological state. In GRMD, attractive harmonic forces are introduced between functional groups that are to react. This might force reactive atoms into each other's vicinity even if they were not without the presence of these forces. On the other hand, this approach shortcuts the required simulation time due to the speed-up of monomer diffusion.

Graph-theoretical studies show that the degree distribution and its evolution directly affect the topological properties of polymer chains and networks, such as the gel point and the weight distribution. From a physical point of view, the degree of a monomer is the property that affects its reactivity the most, other than the actual chemical reaction probability between the specific functional groups in the system. As our results show, the degree distributions from RMD, GRMD and theoretical models match over the whole of the polymerisation process, meaning that the GRMD protocol can be used as an efficient, yet accurate substitute to simulate polymer network formation for systems in which the functional group reactivities on a monomer are independent.

The GRMD protocol was used to construct virtual samples of a family of compound materials used in 3D printing, consisting of BDM, DBA and NVP monomers; the first two of which form crosslinked polymer networks, while the latter undergoes free radical polymerisation resulting in long polymeric chains.

Due to the fact that in reactive MD simulations, one can keep record of the precise bonding history, the cluster size evolution of the different coexisting materials was easily computed. Furthermore, physical measurements can also be performed in the virtual environment. Dilatometric and tensile experiments were performed on each simulated material, to find their shrinkage upon crosslinking, the glass transition temperature, the yield stress and the Young's modulus. The glass transition temperature and the Young's modulus were compared to experimental results on the same

materials, using values from Ref.[7]

It was found that the latter shows no systematic change with the NVP content, and the values are a factor of 3 lower than expected. This can be due to a number of factors, but it is expected that the orders of magnitude higher stretching rate plays the largest role. The full relaxation used in simulation between strain increments could also fail to reproduce results, as in a realistic, hard material, the bulk is confined by its outer layers, altering its mechanical properties.

For the glass transition temperature (T_g), the similar trend was found as in experimental studies. The T_g of pure BMI (BDM/DBA monomers) is much higher than of the compound materials, which show small variation with NVP content until the mass ratio of matrix (BDM/DBA) and NVP monomers in the system are similar. In this case, T_g starts to approach the value found for pure NVP. The initial small deviation with rising NVP content, and the larger drop above a threshold, can be explained by looking at the cluster size evolution. At the end of the polymerisation process, the material with the highest NVP content shows similar weight average molecular size, but lower number average size. This can be related to the existence of small molecules, possibly monomers at the end of the curing. This indicates that the higher NVP content not only pushes the physical properties of the compound material towards of the pure NVP's, but also affects the evolution of the BMI network, e.g. by the caging of some BDM/DBA monomers which are then not incorporated in the gelled macromolecule, lowering the glass transition temperature.

The effect of much smaller time and length-scales of MD simulations compared to experiments also manifested themselves in the T_g measurements, but using the extrapolation theories based on the WLF and Flory-Fox equations, these could be accounted for, and the actual T_g calculated was close to expected.

Finally, the volume shrinkage upon crosslinking was predicted accurately, indicating that the COMPASS III force field can perform well on models of polymer systems.

To summarise, it was shown that the GRMD protocol can be an accurate and efficient tool to construct polymer networks for molecular modelling. Whilst the number of the accurately predictable properties might currently be limited, it is possible to predict some important physical properties of the simulated material using the

constructed networks.

5. Conclusions

Two protocols have been described that are used for simulating polymer chain and network formation in a Molecular Dynamics (MD) environment: Reactive Molecular Dynamics (RMD) and Guided Reactive Molecular Dynamics (GRMD). The GRMD protocol and the COMPASS III force field were used to construct virtual samples of a set of BMI/NVP composite materials used in 3D printing. The monomers in this process undergo free radical reactions and various step-growth polymerisation reactions. It has been shown that the GRMD protocol reproduces the results of the more expensive RMD simulations for monomers, for systems where the functional group reactivity is independent of the monomer degree.

The simulation of the curing process for systems consisting of 610 monomers resulted in a speed up of a factor of 6 when using the guided approach. These samples were subjected to physical measurements using MD, which showed agreement for the glass transition temperature with experimental data. The methods presented show good potential in the molecular modelling of polymerisation with efficiency that allows the construction of polymer networks consisting of hundreds of monomers in reasonable time. This allows the prediction of properties of large numbers of samples that are essential for industrial application.

Acknowledgements

This work was supported by the Engineering and Physical Sciences Research Council (EPSRC) through an Industrial Cooperative Awards in Science & Technology (iCASE) studentship [grant number LJAM/084].

Appendix A. Glass transition temperature fit procedure

To obtain the glass transition temperature T_g we assume that the thermal expansion α is sigmoidal in temperature T, specifically a hyperbolic tangent of the reduced

temperature $\theta = (T - T_g)/T_0$,

$$\alpha = \mu + \sigma \tanh\theta \tag{A1}$$

where μ is the thermal expansion at the glass transition, and σ the deviation from the average, such that in the glass state the thermal expansion is $\mu - \sigma$, rising to $\mu + \sigma$ in the rubber state. The scaling factor T_0 determines the width of the transition.

The thermal (volume) expansion is related to volume by

$$\alpha = \frac{1}{V}\left(\frac{\partial V}{\partial T}\right)_{N,p} = \frac{1}{T_0}\left(\frac{\partial \ln V}{\partial \theta}\right)_{N,p}$$

Substituting Eq. (A1), and integrating over θ we obtain

$$\begin{aligned} \ln\frac{V}{V_g} &= \int_0^\theta d\theta\, T_0\,(\mu + \sigma\tanh\theta) \\ &= T_0\,(\mu\theta + \sigma \ln\cosh\theta) \end{aligned}$$

where V_g is the volume at the glass transition. Rearranging it follows that

$$V = V_g\, e^{\mu(T-T_g)} \cosh^{\sigma T_0}\left(\frac{T - T_g}{T_0}\right)$$

Given a set of data points (V_i, T_i) with uncertainties (σ_i, T_i) we can obtain the parameters V_g, T_g, T_0, μ, and σ by minimising $\sum_i \left(\frac{V_i - V(T_i)}{\sigma_i}\right)^2$. The minimisation is carried out using the Levenberg-Marquardt algorithm. The obtained T_g values were extrapolated using the Williams-Landel-Ferry (WLF) and Flory-Fox equations to account for the orders of magnitudes higher cooling rate, and finite molecular sizes in MD simulations.

The estimated T_g value using the WLF equation is given by

$$T_g^{WLF} = T_g + \frac{C_2 \log\left(q_{real}/q_{sim}\right)}{C_1 + \log\left(q_{real}/q_{sim}\right)} \tag{A2}$$

where T_g is the glass transition temperature found using the dilatometric simulations,

$C_1 = 17.44$ and $C_2 = 51.6$ K, as suggested for polymers[27], and q_{real} and q_{sim} denotes the cooling rates in a realistic case and as set in the simulation respectively. For the former, a value of 20 K/min was chosen, while the latter is determined by simulation settings, with a value of 0.2 K/ps. The experimental M_n and M_w values are estimated to be 200 times of molecules in the model.

The obtained T_g^{WLF} value is further extrapolated using the Flory-Fox equation

$$T_{g,final} = T_g^{WLF} - K\left(\frac{1}{\sqrt{M_n^{exp} M_w^{exp}}} - \frac{1}{\sqrt{M_n^{sim} M_w^{sim}}}\right) \tag{A3}$$

where the geometric mean of the number average molecular weight M_n, and the weight average molecular weight M_w is used. The coefficient K is estimated to have a value of $3\text{x}10^5$, following Bicerano's estimation and using an expected glass transition temperature of 480 K. For the case of NVP, instead of the geometric mean, it is simply the number average molecular weight that is used, since a narrower molecular weight distribution is expected, contrary to the BMI co-polymers, where the finite NVP chains and the massive BMI macromolecules result in a wide distribution.

Appendix B. Reaction definition in RMD and GRMD

The *Reactive Molecular Dynamics* and *Guided Reactive Molecular Dynamics* protocols utilise the GUI of Materials Studio, so that is possible to simply define chemical reactions. The user has to draw molecular fragments that participate in the given reaction, and define seven sets consisting of atoms and/or bonds as described below, and shown in Fig. B1 displaying the reaction definition file for the Diels-Alder reaction.

In the file, the product fragment has to be sketched, with bonds that break also included (no such bond is present for the Diels-Alder reaction). The first four sets to be defined are the reacting fragments on both reactant molecules, and the one reaction atom on each fragment, for which the cutoff criterion is checked. The protocol uses element based pattern match that finds all fragments in the system with the specified atomic topology. The next two sets are simply the bonds that form, and the ones that break in the reaction. Finally, a set is defined for atoms that cannot participate

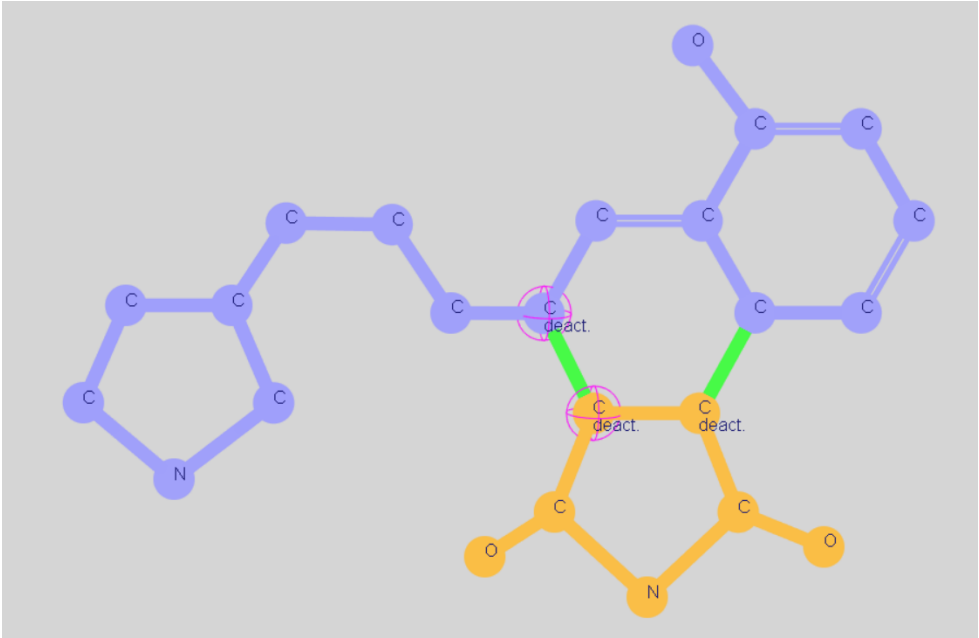

Figure B1.: Definition of the Diels-Alder reaction in the RMD and GRMD protocols. The fragments of the molecules participating in the reaction are sketched. The user has to define seven sets: two reactant fragments (blue and orange), two reaction atoms (in cages), bonds to be added (green), bonds to be deleted (not present for this reaction), and atoms that cannot participate in further reactions (named "deact.").

in further reactions, such as the reaction atoms. Note that in Fig. B1, both carbon atoms of the DBA fragment are labelled as deactivated, because of symmetry. As the protocol performs a pattern match based on element types, and bonding information is not taken into consideration, if reacted atoms are not set to deactivated, they may form further, unphysical bonds with other BDM/DBA chain fragments.

Finally, hydrogen atoms are not included in the sketch, as these are deleted and added automatically for each atom that is part of the reacting fragments, once the intermediate state has formed.

References

[1] Lei D, Yang Y, Liu Z, et al. A general strategy of 3D printing thermosets for diverse applications. Mater Horiz. 2019;6:394–404.

[2] Tseng JW, Liu CY, Yen YK, et al. Screw extrusion-based additive manufacturing of peek. Materials & Design. 2018;140:209 – 221.

[3] Guo Y, Ji Z, Zhang Y, et al. Solvent-free and photocurable polyimide inks for 3D printing.

J Mater Chem A. 2017;5:16307–16314.

[4] Shi Q, Yu K, Kuang X, et al. Recyclable 3D printing of vitrimer epoxy. Mater Horiz. 2017;4:598–607.

[5] Compton BG, Lewis JA. 3D-printing of lightweight cellular composites. Advanced Materials. 2014;26(34):5930–5935.

[6] Wallin TJ, Pikul J, Shepherd RF. 3D printing of soft robotic systems. Nature Reviews Materials. 2018;3:84–100.

[7] Wu T, Jiang P, Zhang X, et al. Additively manufacturing high-performance bismaleimide architectures with ultraviolet-assisted direct ink writing. Materials & Design. 2019; 180:107947.

[8] Gouzman I, Atar N, Grossman E, et al. 3D printing of bismaleimides: From new ink formulation to printed thermosetting polymer objects. Advanced Materials Technologies. 2019;4(10):1900368.

[9] Wagner A, Gouzman I, Atar N, et al. Cure kinetics of bismaleimides as basis for polyimide-like inks for polyjet^{TM}-3D-printing. Journal of Applied Polymer Science. 2019; 136(12):47244.

[10] Rau DA, Herzberger J, Long TE, et al. Ultraviolet-assisted direct ink write to additively manufacture all-aromatic polyimides. ACS Applied Materials & Interfaces. 2018; 10(41):34828–34833.

[11] Zhang W, Qing Y, Zhong W, et al. Mechanism of modulus improvement for epoxy resin matrices: A molecular dynamics simulation. Reactive and Functional Polymers. 2017; 111:60–67.

[12] Zhang W, Li H, Gao L, et al. Molecular simulation and experimental analysis on thermal and mechanical properties of carbon nanotube/epoxy resin composites with different curing agents at high-low temperature. Polymer Composites. 2018;39(S2):E945–E954.

[13] Wang Z, Lv Q, Chen S, et al. Glass transition investigations on highly crosslinked epoxy resins by molecular dynamics simulations. Molecular Simulation. 2015;41(18):1515–1527.

[14] Yang Q, Li X, Shi L, et al. The thermal characteristics of epoxy resin: Design and predict by using molecular simulation method. Polymer. 2013;54(23):6447–6454.

[15] Fu K, Xie Q, Lü F, et al. Molecular dynamics simulation and experimental studies on the thermomechanical properties of epoxy resin with different anhydride curing agents. Polymers. 2019;11(6):975.

[16] Akkermans RLC, Spenley NA, Robertson SH. Monte Carlo methods in Materials Studio.

Molecular Simulation. 2013;39(14-15):1153–1164.

[17] Li C, Strachan A. Molecular simulations of crosslinking process of thermosetting polymers. Polymer. 2010;51(25):6058–6070.

[18] Varshney V, Patnaik SS, Roy AK, et al. A molecular dynamics study of epoxy-based networks: cross-linking procedure and prediction of molecular and material properties. Macromolecules. 2008;41(18):6837–6842.

[19] Akkermans RL, Toxvaerd S, Briels WJ. Molecular dynamics of polymer growth. The Journal of chemical physics. 1998;109(7):2929–2940.

[20] Yarovsky I, Evans E. Computer simulation of structure and properties of crosslinked polymers: application to epoxy resins. Polymer. 2002;43(3):963–969.

[21] Kryven I, Duivenvoorden J, Hermans J, et al. Random graph approach to multifunctional molecular networks. Macromolecular Theory and Simulations. 2016;25(5):449–465.

[22] Kryven I, Iedema PD. Predicting multidimensional distributive properties of hyperbranched polymer resulting from AB2 polymerization with substitution, cyclization and shielding. Polymer. 2013;54(14):3472–3484.

[23] Kryven I, Iedema PD. Transition into the gel regime for crosslinking radical polymerisation in a continuously stirred tank reactor. Chemical Engineering Science. 2015;126:296–308.

[24] Kryven I. Analytic results on the polymerisation random graph model. Journal of Mathematical Chemistry. 2018;56(1):140–157.

[25] Souza I, Martins J. Metric tensor as the dynamical variable for variable-cell-shape molecular dynamics. Phys Rev B. 1997 Apr;55:8733–8742.

[26] Radue MS, Varshney V, Baur JW, et al. Molecular modeling of cross-linked polymers with complex cure pathways: a case study of bismaleimide resins. Macromolecules. 2018; 51(5):1830–1840.

[27] Williams ML, Landel RF, Ferry JD. The temperature dependence of relaxation mechanisms in amorphous polymers and other glass-forming liquids. Journal of the American Chemical society. 1955;77(14):3701–3707.

[28] Ogawa T. Effects of molecular weight on mechanical properties of polypropylene. Journal of applied polymer science. 1992;44(10):1869–1871.